npj | precision oncology

Article

Published in partnership with The Hormel Institute, University of Minnesota

https://doi.org/10.1038/s41698-026-01414-0

Validation of QuANTUM-derived tumor cell fraction for molecular testing in high-grade serous tubo-ovarian carcinoma

Antonio Maria Alviano[1,2], Fabio Pagni[1,2], Davide Seminati[2], Gabriele Casati[1,2], Marta Jaconi[2], Robert Fruscio[1,3], Antonio De Leo[4], Thais Maloberti[5], Vincenzo L'Imperio[1,2], Dario De Biase[5] & Giorgio Cazzaniga[1,2] ✉

Tumor cell fraction (TCF) estimation is an essential step in homologous recombination deficiency (HRD) testing of tubo-ovarian high-grade serous carcinoma (HGSC). However, it is prone to variability and observer dependence. Here, we assess the reliability of the QuANTUM computational pipeline for TCF estimation (cTCF) in HGSC samples. 70 HGSC cases were retrospectively collected and the AmoyDx HRD Focus Panel was employed for DNA extraction and sequencing. TCF estimates were obtained from multiple pathologists, along with the TCF calculated by the proprietary AmoyDx algorithm. The QuANTUM pipeline-derived cTCF and a manually calculated ground truth (GT) were obtained on the same slides, and concordance analyses were performed. Weighted kappa (*Wk*) values for the agreement among the various pathologists ranged from 0.28 to 0.63, reflecting low to substantial concordance. The QuANTUM algorithm showed substantial and better agreement with the GT and the AmoyDx tool (*Wk* = 0.73 and 0.63, respectively) as compared to the pathologists' estimates. No significant differences were observed between QuANTUM, the GT and the AmoyDx tool in identifying cases with tumor cellularity above or below the method-defined 30% cutoff. Considering its high reliability, the QuANTUM algorithm may serve as a robust tool for ensuring adequate TCF evaluation in HGSC.

High-grade serous carcinoma (HGSC) is the most common tubo-ovarian malignancy, accounting for approximately 320,000 new cases and 200,000 deaths per year worldwide[1]. Cytoreductive surgery and platinum- and taxane-based chemotherapy (with or without bevacizumab) represent the mainstays of treatment for advanced-stage HGSC, achieving a 5-year survival rate of only 30–40%[2].

Over the past decade, the therapeutic landscape of this cancer has been revolutionized by the introduction of poly-(ADP ribose) polymerase inhibitors (PARPis), which exploit the synthetic lethality resulting from the dysfunction of the homologous recombination repair (HRR) complex in cancer cells[3]. In this context, the identification of homologous recombination deficient (HRD) tumors has become a cornerstone of clinical management. While PARPi efficacy has been observed across broader populations, including those with homologous recombination proficient (HRP) status in certain settings, the magnitude of benefit is significantly greater in HRD-positive cases. Consequently, for several clinical indications, HRD testing is not only a predictive tool but a regulatory requirement to determine patient eligibility and enable access to therapy[4].

HRD can result from several mechanisms, including loss-of-function mutations in the BRCA1 or BRCA2 tumor-suppressor genes, BRCA1/2 promoter hypermethylation, and aberrations in other HRR genes (e.g., RAD methylation) or genes whose protein products interact with BRCA1/2 (e.g., EMSY)[5,6]. Of note, germline and somatic BRCA1/2 mutations appear to have comparable effects in terms of sensitivity to PARPi-based therapy[7].

The most widely employed molecular assays to determine tumor HRD status typically combine BRCA1/2 mutation testing with the detection of genomic effects secondary to HRD (so-called "genomic scars")[8–12]. To correctly assess tumor HRD status, these tests require the tumor cell fraction

[1]Department of Medicine and Surgery, University of Milano-Bicocca, Monza, Italy. [2]Pathology, Fondazione IRCCS San Gerardo dei Tintori, Monza, Italy. [3]UO Gynecology, Fondazione IRCCS San Gerardo dei Tintori, Monza, Italy. [4]Department of Experimental, Diagnostic and Specialty Medicine, University of Bologna-Molecular Diagnostic Unit, Azienda USL di Bologna, Bologna, Italy. [5]Solid Tumor Molecular Pathology Laboratory, IRCCS Azienda Ospedaliero-Universitaria di, Bologna, Bologna, Italy.
✉e-mail: g.cazzaniga18@campus.unimib.it

THE HORMEL INSTITUTE
UNIVERSITY OF MINNESOTA

(TCF) to exceed a certain threshold, therefore TCF determination has become a key part of the histopathological evaluation of HGSC samples[13]. This task, often performed by a single experienced pathologist, typically results in a repetitive, laborious, and observer-dependent operation[14].

Therefore, a growing body of research is investigating the opportunity of employing computational methods to streamline the assessment of tumor sample adequacy for molecular analyses[15]. Our group has developed and tested a computational algorithm known as the QuPath Analysis of Nuclei from Tumor to Uniform Molecular test (QuANTUM) pipeline, which demonstrated excellent reliability compared to the ground truth (GT) in the assessment of TCF from lung cancer cases[16]. However, the broader application of this pipeline to other cancer types, including tubo-ovarian HGSC, still needs to be investigated.

Here, we assess the reliability of the QuANTUM pipeline on 70 HGSC samples, with a specific focus on specimens with TCFs near the molecular panel adequacy threshold for tumor cellularity. Our aim is to investigate whether this computational pathology tool could be implemented in the routine pathology workflow to optimize the evaluation of tubo-ovarian HGSC cases undergoing molecular analyses.

Results

Histopathologic and molecular features of the study cohort

A total of 70 tubo-ovarian HGSC cases were included in the study. The specific characteristics of the cohort are reported in Supplementary Table S1. Most specimens were obtained from uterine adnexa (46 cases), followed by omentum/mesentery/peritoneum (11 cases), uterus (9 cases), lymph nodes and abdominal wall (2 cases each). Surgical samples were the most common type of specimen ($n = 48$, 68.57%), followed by frozen sections ($n = 13$, 18.57%) and biopsies ($n = 9$, 12.86%). The distribution of TCF values according to the GT is reported in Supplementary Fig. S1. The mean TCF of biopsy samples was significantly lower than that of frozen sections ($p = 0.002$) and surgical specimens ($p = 0.012$).

15 cases (21.43%) were found to carry BRCA1/2 mutations, while 55 (78.57%) were BRCA-wild-type (WT). Regarding HRD status, 39 cases (55.71%) were HRD-positive (GSS ≥ 50), while 31 (44.29%) were HRD-negative (GSS < 50). All BRCA1/2-mutated samples were HRD-positive, except for one case carrying a *BRCA1* class 3 (VUS, variant of uncertain significance) mutation and showing a GSS of 29.

No statistically significant differences were noted between the two institutions that provided the samples analyzed in the study.

Pathologists' agreement on pTCF

Varying levels of agreement were found between the six human observers regarding pTCF estimation: *Wk* values ranged from 0.28 to 0.63, while ρ values ranged from 0.47 to 0.88, reflecting fluctuating inter-rater reliability and emphasizing inconsistencies between raters (Table 1, Fig. 1). As for the concordance with the GT, the *Wk* values highlighted partial inconsistencies, showing limited agreement when considering a single observer. Specifically, the mean absolute error (MAE) values relative to the GT were as follows: original rater (14.74 ± 1.44%), pathologist #1 (5.29 ± 3.51%), pathologist #2 (6.79 ± 5.64%), pathologist #3 (6.79 ± 5.64%), pathologist #4 (16.79 ± 5.64%), and pathology resident (6.79 ± 1.44%). The agreement progressively improved when averaging multiple raters. While the comparison between the mean rating of a single observer and the GT yielded a *Wk* range of 0.40–0.59 (confidence interval [CI]: 0.23–0.70), this agreement index increased to 0.49-0.67 (CI: 0.33–0.78), 0.54-0.69 (CI: 0.41–0.79), 0.59–0.69 (CI: 0.45–0.79), and 0.60–0.68 (CI: 0.47–0.78) when considering the mean of 2, 3, 4, or 5 raters, respectively. Notably, the level and the field of expertise did not impact the agreement, suggesting that consistency arises primarily from averaging multiple evaluations rather than individual proficiency.

cTCF assessment through the QuANTUM pipeline

The computational pipeline showed substantial agreement with the GT ($Wk = 0.73$, $\rho = 0.91$) and satisfactory concordance with the mean pathologists' and AmoyDx TCFs ($Wk = 0.70$, $\rho = 0.87$ and $Wk = 0.63$, $\rho = 0.84$, respectively). In turn, the AmoyDx estimations showed substantial agreement with the GT ($Wk = 0.63$, $\rho = 0.85$) and the mean pTCF of the six raters ($Wk = 0.58$, $\rho = 0.79$). No statistically significant differences were noted between these four methods (i.e., QuANTUM pipeline, pTCF estimation, AmoyDx tool, and GT) in terms of TCF determination, further confirming their similar performances (Table 2, Fig. 2).

The validation of the cTCF method was conducted on 10 randomly selected WSIs, independently assessed by three different raters (i.e., validators #1 [DS] and #2 [GC] and the pathology resident who annotated the entire WSI set for cTCF estimation). Substantial interobserver agreement was noted, with *Wk* values ranging from 0.60 to 0.64. Additionally, the lack of statistically significant differences between raters indicated that operator variability does not significantly impact the reproducibility of cTCF estimation.

TCF estimation and HRD status determination in cases with borderline tumor cellularity

Considering the recommended threshold for molecular analyses through the AmoyDx platform, namely a TCF ≥ 30%[17], we assessed the performance of the QuANTUM pipeline in discriminating between samples with adequate (i.e., ≥ 30%) vs. low (i.e., < 30%) tumor cellularity. The QuANTUM algorithm showed a substantial concordance with the GT ($k = 0.75$) and an excellent agreement with the mean pTCF ($k = 0.83$) and the AmoyDx tool ($k = 0.88$) (Table 3). Specifically, our computational pipeline had the second-to-lowest absolute disagreement rate (ADR) with the GT (ADR = 5.71%), being outperformed only by the AmoyDx test (ADR = 2.88%). Among human observers, the ADR values with the GT were equal or higher than those of the QuANTUM algorithm (7.14%, 14.29%, 8.57%, 8.57%, 10%, and 5.71% for original rater, pathologists #1, #2, #3 and #4 and pathology resident, respectively).

There were four discordant cases between the QuANTUM algorithm and the GT regarding the 30% TCF threshold, as well as two discordant cases between QuANTUM and the AmoyDx tool. In all these cases, the computational estimation yielded a tumor cellularity < 30%, while the GT and AmoyDx TCFs were ≥ 30%. The TCF values showed an average difference of 8.5%, ranging from 4% to 12%. There were four discordant cases also between QuANTUM and the mean pTCF, with two cases shifting from < 30% to ≥ 30% and the other two in the opposite direction. The average TCF difference in these cases was slightly higher (mean: 10.8%, range: 3–20%).

Considerable differences were found in the proportion of HRD-positive cases within adequately cellular samples compared to cases with low TCF values. Specifically, 38 out of 62 cases (61.3%) with adequate cellularity (i.e., a GT TCF ≥ 30%) were HRD-positive, compared to only 1 out of 8 samples (12.5%) with suboptimal cellularity. Of note, all these 8 cases had a TCF < 30% also, according to the QuANTUM algorithm and the AmoyDx tool. A similar trend was observed with BRCA-mutated cases, whereby all the 15 BRCA mutations identified in the analyses occurred in samples with adequate cellularity (Fig. 3).

Performance of the QuANTUM algorithm in challenging cases

To investigate the potential of our computational tool to assist pathologists with TCF estimations in challenging cases, we focused on samples with the lowest agreement among the six human observers. Specifically, we considered all cases where at least one rater pair showed a difference between their TCF estimates ≥ 30% (i.e., the 90th percentile of the absolute TCF differences among all rater pairs). Within the 39 samples meeting these criteria, the proportion of surgical specimens, frozen sections, and biopsies was 66.67%, 15.38% and 17.95%, respectively, which was comparable to that of the original cohort (p = 0.297). The mean pTCF of this subgroup showed a substantial agreement with the GT ($Wk = 0.74$, $\rho = 0.73$), confirming that averaging multiple observers enables to limit the impact of inter-rater discrepancies. However, the concordance between QuANTUM and the GT was excellent ($Wk = 0.91$, $\rho = 0.87$), reflecting the superior performance of

Table. 1 | Inter-observer agreement and correlation for TCF assessment

GT	1	ρ 0.47 ***	ρ 0.81 ***	ρ 0.67 ***	ρ 0.74 ***	0.75 ***	0.79 ***
pTCF Original	*Wk* 0.50 [0.26–0.68] -	1	ρ 0.48 ***	ρ 0.47 ***	ρ 0.68 ***	ρ 0.56 ***	ρ 0.65 ***
Path #1	*Wk* 0.75 [0.63–0.85] -	Wk 0.34 [0.21–0.47] *	1	ρ 0.88 ***	ρ 0.79 ***	ρ 0.64 ***	ρ 0.76 ***
Path #2	*Wk* 0.69 [0.54–0.81] -	*Wk* 0.28 [0.15–0.40] ***	*Wk* 0.63 [0.53–0.72] -	1	ρ 0.72 ***	ρ 0.65 ***	ρ 0.74 ***
Path #3	*Wk* 0.71 [0.58–0.82] -	*Wk* 0.48 [0.36–0.60] **	*Wk* 0.48 [0.35–0.60] -	*Wk* 0.49 [0.36–0.61] -	1	ρ 0.74 ***	ρ 0.79 ***
Path #4	*Wk* 0.71 [0.57–0.81] -	*Wk* 0.35 [0.22–0.47] ***	*Wk* 0.49 [0.38–0.60] -	*Wk* 0.50 [0.37–0.62] -	*Wk* 0.52 [0.41–0.62] -	1	ρ 0.80 ***
Resident	*Wk* 0.79 [0.68–0.86] -	*Wk* 0.51 [0.36–0.63] -	*Wk* 0.52 [0.39–0.63] -	*Wk* 0.44 [0.32–0.55] **	*Wk* 0.52 [0.43–0.61] **	*Wk* 0.44 [0.32–0.55] *	1
	GT	**pTCF Original**	**Path #1**	**Path #2**	**Path #3**	**Path #4**	**Resident**

The upper-right triangle of the matrix displays the Spearman's correlation coefficients (ρ), while the lower-left triangle presents the Weighted Kappa (*Wk*) values for each pair of observers
*$p < 0.05$; **$p < 0.01$; ***$p < 0.001$. *GT* ground truth, *Path* pathologist, *pTCF* pathologist tumor cell fraction, *TCF* tumor cell fraction.

our algorithm in challenging scenarios. Finally, a review of these cases revealed that most of the observed discrepancies were attributable to the scoring of tumor cellularity in the proximity of necrotic areas and/or regions with prominent immune cell infiltration. Substantial disagreement was also noted in the assessment of atypical cells at the interface between tumor nests and the surrounding stroma, particularly in cases with a predominant solid pattern (Fig. 4).

Discussion

Targeted therapies have revolutionized the field of oncology, yielding remarkable survival benefits in numerous cancer types[18]. Consequently, predictive biomarker testing has become an integral part of the diagnostic workflow of several malignancies, including tubo-ovarian HGSC, where HRD testing is recommended in all patients with advanced-stage (i.e., Fédération Internationale de Gynécologie et d'Obstétrique [FIGO] stage ≥ III) disease to predict the magnitude of benefit from PARPis[19,20]. The pathologist plays a key role in this process, being responsible for proper tissue handling, selection of tumor tissue area, and estimation of the TCF for subsequent molecular assays[21]. Ensuring accurate and reproducible TCF estimation is of paramount importance for the success of HRD tests, since gene variant calling and "genomic scar" detection through molecular techniques require a tumor cellularity above a prespecified threshold to ensure test reliability[11,17,22]. Inaccurate TCF determination may thus lead to inconclusive or even misleading results, with a negative impact on patient management and healthcare costs[23].

Considering the well-known intra- and interobserver variability associated with visual estimates of histopathological parameters[24,25], several computer-aided diagnostic (CAD) tools have been developed to support pathologists in routine tasks requiring cell counting and/or tissue area estimation, such as Ki-67 scoring[26], Gleason grading[27], and more recently, TCF determination[28]. Our group has developed a semi-automated algorithm for TCF estimation known as the QuANTUM pipeline, which showed excellent reliability compared to the GT in lung cancer WSIs, providing an easily accessible and relatively inexpensive tool to support pathologists in this tedious and repetitive task[16]. However, the potential application of our digital pathology platform to other cancer types has since remained unexplored. Here, we assessed the performance of the QuANTUM pipeline in the setting of tubo-ovarian HGSC, with a specific focus on the potential impact of this computational method on BRCA1/2 and HRD testing results.

We observed substantial agreement between the QuANTUM algorithm and the GT, thus confirming its reliability and encouraging further studies to validate its use in other malignancies. Our computational tool also showed satisfactory concordance with the automated TCF estimation by the AmoyDx HRD assay and with the mean TCF of the six pathologists. Interestingly, the agreement between QuANTUM and the GT was higher than that of any individual rater, irrespective of their level of experience.

As reported in previous works[16,28,29], TCF estimations for a given sample by the six scorers were highly variable, as were the interobserver concordance values for the various rater pairs, ranging from "poor" to "substantial". Increasing the number of observers improved the agreement with the GT, as indicated by the progressively narrower CIs of the corresponding *Wk* values. Thus, the assessment of a given sample by multiple raters may improve the accuracy of TCF estimation, which could be particularly valuable in borderline cases to guide the selection of suitable samples and slides for molecular analysis.

Given that our semi-automated method requires manual annotations of malignant and non-neoplastic elements on WSIs, we asked whether human subjectivity in annotating the digital slides could introduce a bias in cTCF estimations. The comparison between the cTCF values obtained by three different annotators on a set of randomly selected cases showed that QuANTUM estimations are not operator-dependent, which is a crucial prerequisite for the broader application of our pipeline across pathology laboratories, and it is consistent with our previous findings[16].

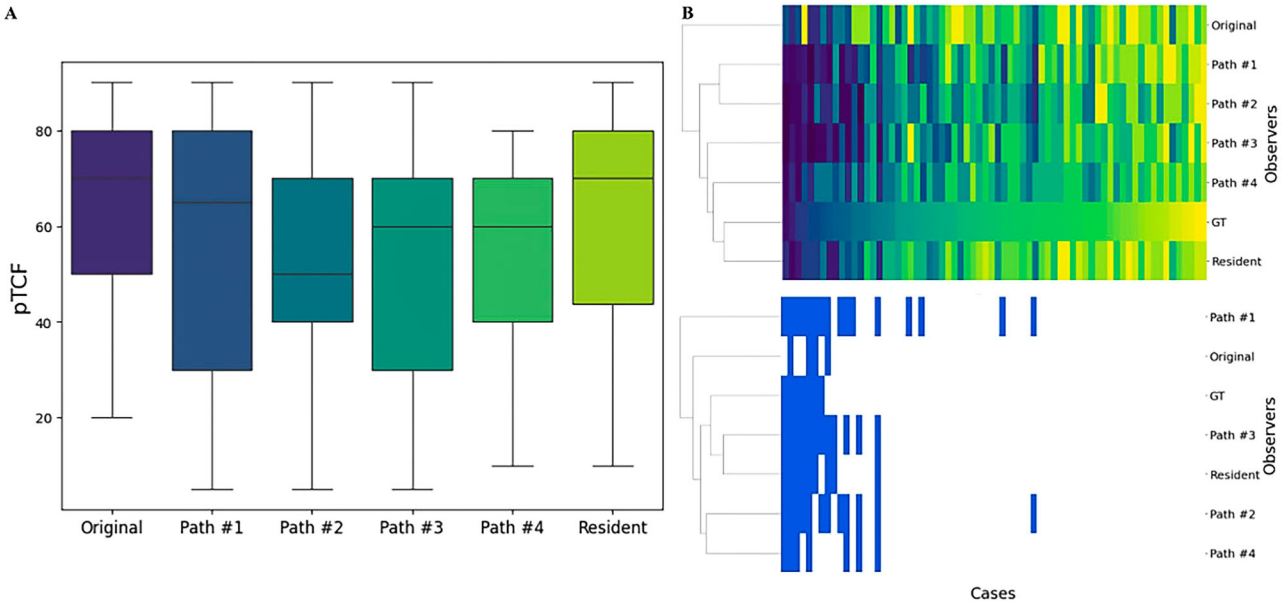

Fig. 1 | pTCF estimation. A Box plots showing the distribution of TCF estimations across different observers. **B** Hierarchical clustering heatmaps of continuous pTCF (top) and categorical pTCF estimations (bottom). Cases are ordered by increasing values of GT TCF. In the top panel, colors range from purple (low cellularity) to light green (high cellularity); in the bottom panel, cases with GT TCF < 30% are represented in blue, while those with GT TCF ≥ 30% are depicted in white. GT ground truth, pTCF pathologist tumor cell fraction, TCF tumor cell fraction.

Table. 2 | Matrix of agreement and correlation for TCF determination across different methods

QuANTUM	1	ρ 0.87	ρ 0.91	ρ 0.84
Mean pTCF	*Wk* 0.70 [0.53–0.87]	1	ρ 0.84	ρ 0.79
GT	*Wk* 0.73 [0.57–0.89]	*Wk* 0.64 [0.46–0.82]	1	ρ 0.85
AmoyDx	*Wk* 0.63 [0.45–0.81]	*Wk* 0.58 [0.38–0.77]	*Wk* 0.63 [0.45–0.81]	1
	QuANTUM	**Mean pTCF**	**GT**	**AmoyDx**

The upper-right triangle displays Spearman's correlation coefficients (ρ), while the lower-left triangle displays Weighted Kappa values (*Wk*)
GT ground truth, *pTCF* pathologist tumor cell fraction, *TCF* tumor cell fraction.

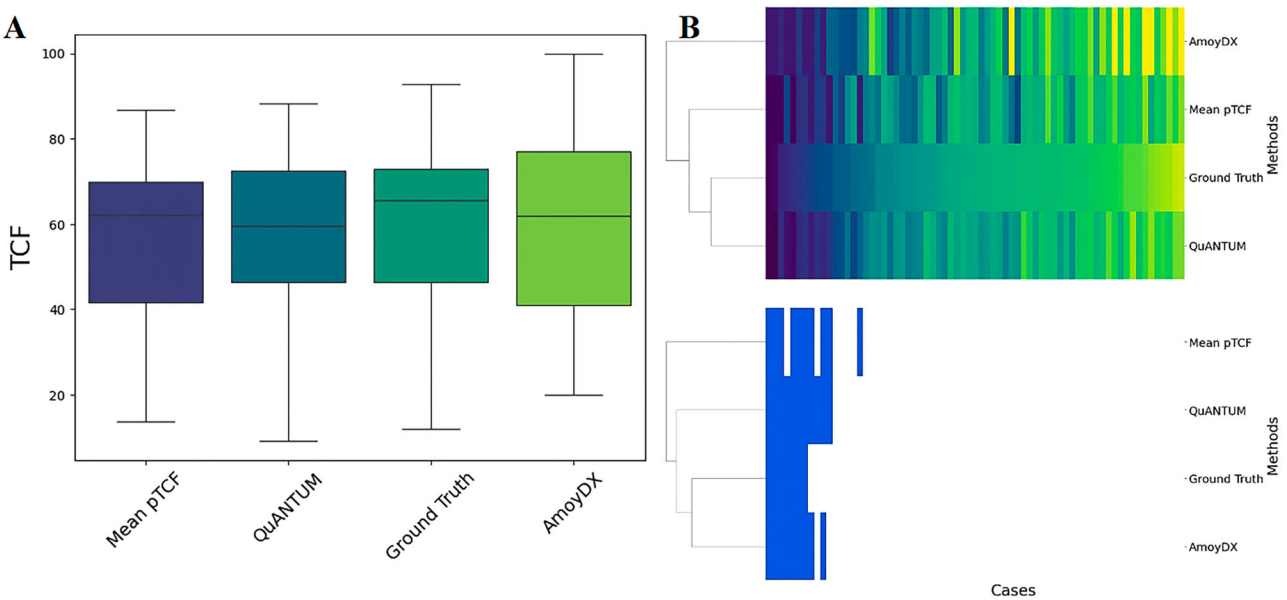

Fig. 2 | Comparison of TCF determinations by different methods. A Box plots showing the distribution of TCF determinations across different methods. **B** Hierarchical clustering heatmaps of continuous TCF (above) and categorical TCF determinations (below). Cases are ordered by increasing values of GT TCF. In the top panel, colors range from purple (low cellularity) to light green (high cellularity); in the bottom panel, cases with GT TCF < 30% are represented in blue, while those with GT TCF ≥ 30% are depicted in white. GT, ground truth; pTCF, pathologist tumor cell fraction; TCF, tumor cell fraction.

When focusing on samples with GT TCF values near the 30% threshold recommended by the HRD test manufacturer, the QuANTUM algorithm demonstrated robust performance, supporting its applicability in cases with borderline tumor cellularity. Specifically, in the four cases with GT cellularity above 30% and cTCF estimates below this threshold, the average difference between the TCF values was relatively small. On the other hand, the TCF difference was higher in the four discordant cases between QuANTUM and the mean pTCF, reflecting a more marked discrepancy between these two methods in borderline scenarios. Since the two samples with cTCFs ≥ 30% but pTCFs < 30% had a GT cellularity above this cutoff, relying only on visual pTCF estimation could have relevant workflow implications.

Another noteworthy observation is that, while the percentage of HRD-positive samples among those with adequate GT and QuANTUM cellularity was generally in line with that reported in the literature (i.e., approximately 50%[19]), only 12.5% of cases with GT and QuANTUM cellularity < 30% were HRD-positive. This highlights the challenge faced by molecular tests in accurately assessing complex genomic scars in samples with a TCF below the validated cutoffs[13]. In such cases, relying on an inaccurate HRD result may further complicate the proper contextualization of BRCA1/2 mutation data and potentially lead to unexpected or conflicting findings. It is important to note, however, that our data are derived from a subgroup consisting of only eight cases, highlighting the need for further validation studies in larger cohorts.

Finally, the analysis of cases with the highest discordance rates among pathologists confirmed that the QuANTUM algorithm retains its robust scoring performance in the presence of extensive necrosis, immune cell infiltration and/or atypical cells at the tumor-stroma interface, scenarios where substantial disagreement was observed in manual assessment.

Table. 3 | Cohen's kappa (*k*) values for the agreement on the categorical TCF determination (i.e., low- vs. adequate cellularity) by different methods

QuANTUM	1			
Mean pTCF	0.83 [0.62–1.0]	1		
GT	0.75 [0.46–0.94]	0.67 [0.33–0.93]	1	
AmoyDx	0.88 [0.7–1.0]	0.82 [0.53–1.0]	0.86 [0.58–1.0]	1
	QuANTUM	**Mean pTCF**	**GT**	**AmoyDx**

GT ground truth, *pTCF* pathologist tumor cell fraction, *TCF* tumor cell fraction.

In summary, we showed that our computational pipeline for TCF estimation holds promise for assisting pathologists also with tubo-ovarian HGSC cases. Given its easy accessibility (the QuPath extension is available at https://github.com/Gizmopath/QuANTUM), user-friendly interface, and seamless integration within the QuPath software, our algorithm may provide a useful tool to optimize the routine workflow of molecular pathology laboratories and, ultimately, the personalized management of patients with tubo-ovarian HGSC.

Methods

Cases and TCF determination

Tubo-ovarian HGSC cases undergoing HRD testing from July 2020 to March 2024 were retrospectively collected from the Oncological Molecular Pathology Unit of Fondazione IRCCS San Gerardo dei Tintori (Monza, Italy) ($n = 50$ samples) and the Molecular Pathology of Solid Tumors Laboratories of IRCCS Policlinico di Sant'Orsola (Bologna, Italy) ($n = 20$ samples). Since the two patient groups were not significantly different in terms of their pathological and molecular features ($p > 0.05$), they were considered as a single cohort ($n = 70$ cases) for subsequent analyses.

For each case, Hematoxylin and Eosin (H&E)-stained glass slides (obtained from formalin-fixed, paraffin-embedded [FFPE] HGSC samples) were originally selected by an expert gynecological pathologist (MJ) to define tumor-containing regions (TCRs) for subsequent tumor macrodissection. At this stage, the same pathologist estimated the tumor cell fraction (pTCF, original) to assess sample adequacy for molecular analyses. Slides were then blindly reviewed by a molecular pathologist (DS [pTCF, path #1]), three general pathologists (GC [pTCF, path #2], ADL [pTCF, path #3] andVL [pTCF, path #4]), and a pathology resident (AMA [pTCF, resident]), for the assessment of pTCF. The retrieved slides were anonymized and scanned with a NanoZoomer S60 scanner (Hamamatsu Photonics K.K., Hamamatsu City, Japan) at 20x magnification (0.4416 µm/pixel). Computational tumor cell fraction (cTCF) was obtained on these whole slide images (WSIs) using QuANTUM, as already described in ref. 16. Briefly, for each WSI the StarDist extension within the QuPath software was used for nuclear detection. Then, manual annotations were performed to assign cells to either the "tumor" or the "non-neoplastic" category. These annotations were used to train the QuPath object classifier algorithm to assign each detected nucleus to the above-mentioned categories. cTCF values were obtained as the ratio between the number of nuclei assigned to the "tumor" category by the object classifier algorithm and the total number of nuclei detected in the corresponding WSI. The reproducibility of the obtained cTCF was assessed on a subset of 10 randomly selected cases, which were independently annotated and analyzed with the QuANTUM

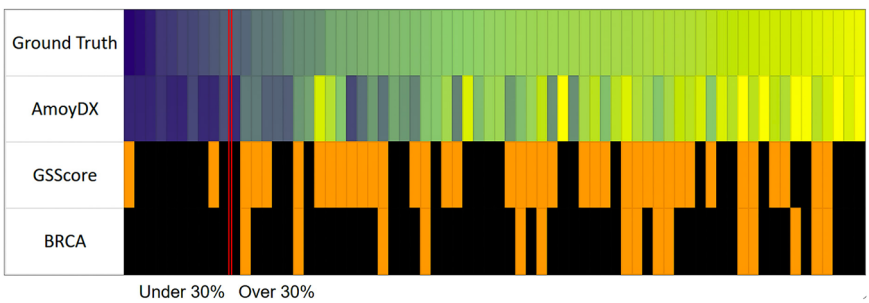

Fig. 3 | TCF determination in cases with borderline tumor cellularity and correlation with the GSS and BRCA mutational status. Top: Heatmaps of the distribution of TCF values according to the manual cell count (i.e., the GT) and the AmoyDx assay. Cases are ordered by increasing values of GT TCF, with colors ranging from purple (low cellularity) to light green (high cellularity). Bottom: HRD-positive cases and those with BRCA mutations are reported in orange, while the remaining cases are shown in black; the red line indicates the 30% TCF cutoff (i.e., the cellularity threshold suggested by the manufacturer as the minimum requirement for diagnostic reliability). A different prevalence of HRD-positive and BRCA-mutated cases was noted in cases with tumor cellularity < 30% compared to those with higher TCF values. GSS genomic scar score, GT ground truth, HRD homologous recombination deficiency, TCF tumor cell fraction.

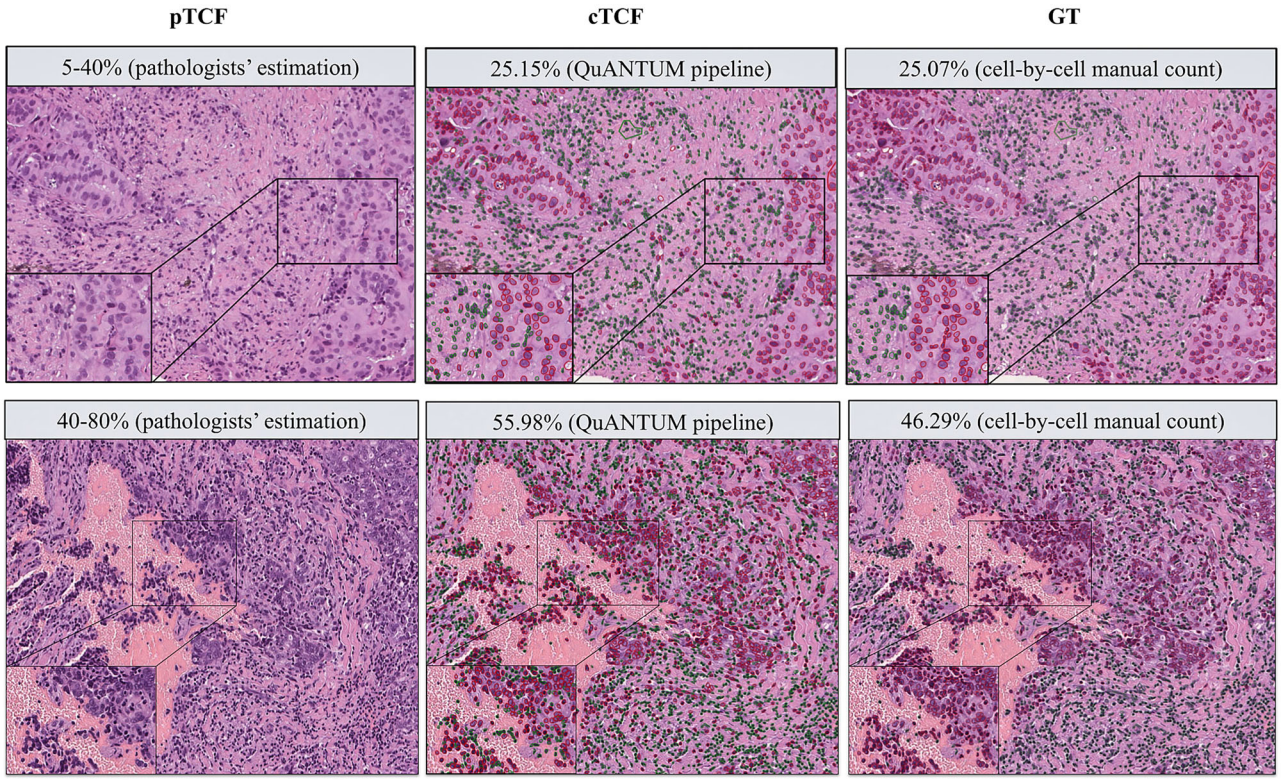

Fig. 4 | Comparison of pTCF, cTCF, and GT tumor cellularity in challenging samples. Shown are two cases for which a significant discordance was noted among pathologists, as well as between the mean pTCF and the GT. On the other hand, the cTCF values provided by the QuANTUM pipeline were comparable with the GT. The top panels show an area where human observers may find it challenging to discriminate malignant cells at the tumor-stroma interface from benign stromal cells, while the bottom panels highlight an area of necrosis. Malignant and non-neoplastic elements are marked in red and green, respectively, while algorithm detections excluded from the total cell count (i.e., tissue elements erroneously identified as cells) are denoted by gray circles (10x magnification; insets: 40x magnification). The reported TCF values refer to the whole slide, not to the ROI shown in the figure. cTCF computational tumor cell fraction, GT ground truth, pTCF pathologist tumor cell fraction, ROI region of interest, TCF tumor cell fraction.

algorithm by two different pathologists (DS [cTCF, validator #1] and GC [cTCF, validator #2]).

To obtain the reference/ground truth (GT) tumor cellularity for each WSI, a cell-by-cell visual count and classification into "tumor" or "non-neoplastic" categories (e.g. immune cells, stromal cells, and normal epithelial cells) was performed after a three-month washout period by the gynecological pathologist (MJ), who was blinded to the results of her initial evaluation.

Molecular analysis

DNA extraction was carried out using the Maxwell® CSC 16 Instrument with the CSC DNA FFPE Kit (Promega, Madison, WI, USA). DNA quantification was performed using the Qubit DNA dsDNA High Sensitivity Assay Kit on a Qubit 4.0 fluorimeter (Thermo Fisher Scientific, Waltham, MA, USA). Templating and sequencing of all samples occurred on the NextSeq 550 System (Illumina, San Diego, CA, USA) using the 300-cycles mid output kit. All samples were analyzed using the AmoyDx HRD Focus Panel assay (Amoy Diagnostics Co., Ltd., Singapore), which enables the preparation of NGS libraries compatible with the previously specified platform and is capable of detecting somatic single nucleotide variants (SNVs) and short insertions and deletions (indels) in the entire coding region and at the intron/exon junctions of the BRCA1 (NM_007294.49) and BRCA2 (NM_000059.3) genes. Additionally, it enables the determination of the Genomic Scar Score (GSS), an algorithmic measure of genomic instability, which is considered positive when it reaches a value ≥ 50.0. The AmoyDx GSS model is based on machine learning and quantifies genomic instability by weighting different types of chromosomal copy number alterations according to their type (i.e., allelic status, whether allele-specific or allele-balanced), length (i.e., small, intermediate or large), and genomic site (i.e., centromeric, telomeric or intrachromosomal), using data from approximately 24,000 single-nucleotide polymorphisms (SNPs) distributed across the whole genome (about 1 SNP per 100 Kb)[8]. All cases with BRCA1/2 mutations classified as class 3, 4, and 5 variants according to the 5-category pathogenicity scheme established by International Agency for Research on Cancer (IARC), American College of Medical Genetics and Genomics (ACMG), and Association for Molecular Pathology (AMP) were considered BRCA-mutated[30,31]. Class 3 variants were included to reflect the total mutational burden detected by the assay, although we acknowledge their uncertain clinical significance. The computational analysis of sequencing data was performed using the AmoyDx ANDAS Data Analyzer software version 1.1.0.230217 (Amoy Diagnostics Co., Ltd.). Data extracted from the computational analysis included the GSS, the mutational status of BRCA1/2 (inclusive of variant allele frequency [VAF], specific site of mutation, mutation type and mutation class), and the tumor cellularity estimated by the device algorithm. In particular, a TCF ≥ 30% was considered as the minimum desirable prerequisite for the reliability of subsequent molecular analyses, as per the manufacturer's instructions[17].

Statistical analysis

Continuous variables were summarized using mean and standard deviation (SD), as applicable, while qualitative variables were reported as counts and frequencies. To compare means and qualitative variables, chi-square tests and Mann-Whitney U tests were employed, depending on the nature of the data. Significance was set at p-values < 0.05 and indicated as '*' for $0.01 < p < 0.05$, '**' for $0.001 < p < 0.01$ and '***' for $p < 0.001$. Cohen's

Kappa (k), Weighted Kappa coefficient (Wk, linear function), and Spearman correlation coefficient (ρ), along with their corresponding p-value, were used to assess the correlation between different observers regarding TCF estimation. Statistical analyses were carried out on Google Colaboratory (Google LLC, Mountain View, CA, USA), using the Python libraries pandas (v. 2.2.2) and scikit-learn (v. 1.6.1).

Ethics approval and consent to participate

The study protocol received approval from the local Ethics Committee (Comitato Etico Brianza, protocol No. 35859, 24/10/22). The study was performed in full accordance with the Declaration of Helsinki.

Data availability

The datasets generated and/or analyzed during the current study are not publicly available as they contain information that could compromise the privacy of research participants, but are available from the corresponding author on reasonable request.

Code availability

The QuANTUM QuPath extension is available at https://github.com/Gizmopath/QuANTUM.

Received: 19 October 2025; Accepted: 29 March 2026;
Published online: 18 April 2026

References

1. Bray, F. et al. Global cancer statistics 2022: GLOBOCAN estimates of incidence and mortality worldwide for 36 cancers in 185 countries. *CA Cancer J. Clin.* **74**, 229–263 (2024).
2. Torre, L. A. et al. Ovarian cancer statistics, 2018. *CA Cancer J. Clin.* **68**, 284–296 (2018).
3. Zheng, F. et al. Mechanism and current progress of Poly ADP-ribose polymerase (PARP) inhibitors in the treatment of ovarian cancer. *Biomed. Pharmacother.* **123**, 109661 (2020).
4. Yi, T. et al. Antitumor efficacy of PARP inhibitors in homologous recombination deficient carcinomas. *Int J. Cancer* **145**, 1209–1220 (2019).
5. Guo, M. & Wang, S. M. The BRCAness landscape of cancer. *Cells* **11**, 3877 (2022).
6. Cousineau, I. & Belmaaza, A. EMSY overexpression disrupts the BRCA2/RAD51 pathway in the DNA-damage response: implications for chromosomal instability/recombination syndromes as checkpoint diseases. *Mol. Genet Genomics* **285**, 325–340 (2011).
7. Hollis, R. L. et al. Somatic BRCA1/2 mutations are associated with a similar survival advantage to their germline counterparts in tubo-ovarian high grade serous carcinoma. *Eur. J. Cancer* **219**, 115299 (2025).
8. Yuan, W. et al. Genomic scar score: A robust model predicting homologous recombination deficiency based on genomic instability. *BJOG* **129**, 14–22 (2022).
9. Roma, C. et al. Harmonization of homologous recombination deficiency testing in ovarian cancer: results from the MITO16A/MaNGO-OV2 trial. *Eur. J. Cancer* **206**, 114127 (2024).
10. Pepe, F. et al. In-house homologous recombination deficiency testing in ovarian cancer: a multi-institutional Italian pilot study. *J. Clin. Pathol.* **77**, 478–485 (2024).
11. Frampton, G. M. et al. Development and validation of a clinical cancer genomic profiling test based on massively parallel DNA sequencing. *Nat. Biotechnol.* **31**, 1023–1031 (2013).
12. Loverix, L. et al. PARP inhibitor predictive value of the Leuven HRD test compared with Myriad myChoice CDx PLUS HRD on 468 ovarian cancer patients from the PAOLA-1/ENGOT-ov25 trial. *Eur. J. Cancer* **188**, 131–139 (2023).
13. Fumagalli, C. et al. In-house testing for homologous recombination repair deficiency (HRD) testing in ovarian carcinoma: a feasibility study comparing AmoyDx HRD Focus panel with Myriad myChoiceCDx assay. *Pathologica* **114**, 288–294 (2022).
14. Smits, A. J. J. et al. The estimation of tumor cell percentage for molecular testing by pathologists is not accurate. *Mod. Pathol.* **27**, 168–174 (2014).
15. Fraggetta, F. et al. Best practice recommendations for the implementation of a digital pathology workflow in the anatomic pathology laboratory by the European Society of Digital and Integrative Pathology (ESDIP). *Diagnostics* **11**, 2167 (2021).
16. L'Imperio, V. et al. Digital counting of tissue cells for molecular analysis: the QuANTUM pipeline. *Virchows Arch.* **486**, 277–286 (2025).
17. Amoy Diagnostics Co., Ltd. AmoyDx® HRD Focus Panel. Datasheet 8.06.0047, ver. B1.1 (2024).
18. Min, H. Y. & Lee, H. Y. Molecular targeted therapy for anticancer treatment. *Exp. Mol. Med.* **54**, 1670–1694 (2022).
19. González-Martín, A. et al. Newly diagnosed and relapsed epithelial ovarian cancer: ESMO Clinical Practice Guideline for diagnosis, treatment and follow-up. *Ann. Oncol.* **34**, 833–848 (2023).
20. Konstantinopoulos, P. A. et al. Germline and somatic tumor testing in epithelial ovarian cancer: ASCO guideline. *J. Clin. Oncol.* **38**, 1222–1245 (2020).
21. Dinneen, K. & Arora, R. Molecular testing in ovarian tumours: challenges from the pathologist's perspective. *Diagnostics* **13**, 2072 (2023).
22. Myriad Genetics, Inc. Myriad myChoice® HRD Technical Specifications. MGL SPEC 022 Rev (2017).
23. Elsea, D. et al. Cost-effectiveness analysis of biomarker testing to guide first-line PARP inhibitor maintenance for patients with advanced ovarian cancer after response to first-line platinum chemotherapy in the USA. *Target. Oncol.* **18**, 531–541 (2023).
24. Turashvili, G. et al. Low interobserver agreement among subspecialised breast pathologists in evaluating HER2-low breast cancer. *J. Clin. Pathol.* **77**, 815–821 (2024).
25. Robert, M. E. et al. High interobserver variability among pathologists using combined positive score to evaluate PD-L1 expression in gastric, gastroesophageal junction, and esophageal adenocarcinoma. *Mod. Pathol.* **36**, 100154 (2023).
26. Alataki, A. et al. A simple digital image analysis system for automated Ki67 assessment in primary breast cancer. *Histopathology* **79**, 200–209 (2021).
27. Pantanowitz, L. et al. An artificial intelligence algorithm for prostate cancer diagnosis in whole slide images of core needle biopsies: a blinded clinical validation and deployment study. *Lancet Digit. Health* **2**, e407–e416 (2020).
28. Frei, A. L. et al. Pathologist computer-aided diagnostic scoring of tumor cell fraction: a Swiss national study. *Mod. Pathol.* **36**, 100335 (2023).
29. Carretero-Barrio, I. et al. Concordance in the estimation of tumor percentage in non-small cell lung cancer using digital pathology. *Sci. Rep.* **14**, 24163 (2024).
30. Plon, S. E. et al. Sequence variant classification and reporting: recommendations for improving the interpretation of cancer susceptibility genetic test results. *Hum. Mutat.* **29**, 1282–1291 (2008).
31. Richards, S. et al. Standards and guidelines for the interpretation of sequence variants: a joint consensus recommendation of the American College of Medical Genetics and Genomics and the Association for Molecular Pathology. *Genet. Med.* **17**, 405–424 (2015).

Acknowledgements

The work has been funded by the project in the Italian Ministry of the University MUR Dipartimenti di Eccellenza 2023-2027 (l. 232/2016, art. 1, commi 314 - 337) and by the National Plan for NRRP Complementary Investments (PNC, established with the decree-law 6 May 2021, n. 59,

converted by law n. 101 of 2021) in the call for the funding of research initiatives for technologies and innovative trajectories in the health and care sectors (Directorial Decree n. 931 of 06-06-2022) - project n. PNC0000003 - AdvaNced Technologies for Human-centrEd Medicine (project acronym: ANTHEM). This work reflects only the authors' views and opinions, neither the Ministry for University and Research nor the European Commission can be considered responsible for them.

Author contributions

A.M.A., Gi.C., and V.L. defined the study design. M.J., D.S., Gi.C., A.D.L., V.L., and A.M.A. performed pTCF estimations. A.M.A., Gi.C., and D.S. applied the computational pipeline for TCF assessment on QuPath. M.J. provided gynecological pathology expert view and performed ground truth determinations. R.F. provided gynecological expert view. D.S. and Ga.C. conducted the molecular analysis and provided molecular pathology expert view. Gi.C. and T.M. performed the statistical analysis. D.D.B., V.L., and F.P. provided funding acquisition and administrative support. All authors were involved in writing the paper and had final approval of the submitted and published versions.

Competing interests

The authors declare no competing interests.

Additional information

Supplementary information The online version contains supplementary material available at https://doi.org/10.1038/s41698-026-01414-0.

Correspondence and requests for materials should be addressed to Giorgio Cazzaniga.